Accident Analysis and Prevention 193 (2023) 107305

Contents lists available at ScienceDirect

Accident Analysis and Prevention

journal homepage: www.elsevier.com/locate/aap

Risk-informed decision-making and control strategies for autonomous vehicles in emergency situations

Hung Duy Nguyen [a,c], Mooryong Choi [b,*], Kyoungseok Han [a,*]

[a] School of Mechanical Engineering, Kyungpook National University, Daegu 41566, South Korea
[b] Nmotion company, Incheon 21984, South Korea
[c] Automation & Control Institute (ACIN), TU Wien, Vienna 1040, Austria

ARTICLE INFO

Keywords:
Autonomous vehicle
Collision avoidance
Decision-making
Finite state machine
Model predictive control
Optimal path planning

ABSTRACT

This paper proposes risk-informed decision-making and control methods for autonomous vehicles (AVs) under severe driving conditions, where many vehicle interactions occur on slippery roads. We assume that the AV should approach a specific safe zone in case of vehicle malfunctioning. In normal situations, the driving behavior of the AV is based on the deterministic finite-state machine (FSM) that makes an appropriate real-time decision depending on the driving condition, which is efficient when compared with some conventional decision-making algorithms; alternatively, in emergency situations, the AV first has to be prevented the rear-end conflicts while the specific safe zone is simultaneously determined by evaluating the level of risk via two safety level indicators, i.e., Time-To-Collision (TTC) and Deceleration Rate to Avoid the Crash (DRAC). The safe path that guides the AV to avoid car crashes is generated based on the trajectory optimization theory (i.e., Pontryagin maximum principle), and the AV follows it based on the linear time-varying model predictive control (LTV-MPC), which ensures the AV's lateral stability. We verify the effectiveness of the proposed decision-making and control strategies in various test scenarios, and the results show that the AV behaves appropriately according to the behaviors of surrounding vehicles and road condition.

1. Introduction

Driving in harsh conditions is dangerous and may lead to fatal accidents. Therefore, it is necessary to recover vehicle stability as soon as possible when the vehicle is about to lose its stability. In addition, hazardous weather conditions, such as extreme snow and rain, are critical factors that cause loss of vehicle yaw stability, especially during the lateral motion of a vehicle. For example, snowfall is one of the most adverse events and poses significant challenges for vehicle control.

A collision avoidance system is considered a central vehicle-safety system for realizing fully autonomous driving. For example, when the AV faces an unexpected dangerous situation, it should move to a safe area while maintaining the vehicle stability. If a collision with an obstacle is inevitable, an appropriate decision should be made to mitigate the damage, and the result should be better than the decision made by most human-drivers in the era of autonomous driving. According to previous research on collision avoidance, changing lanes and lane merging account for approximately 5% of total accidents and 7% of total accident related deaths (Hou et al., 2015). Further, more than 60% of highway traffic accidents involve obstacle avoidance (Pande and Abdel-Aty, 2006).

Motivated by these, we develop a risk-informed decision-making and control strategy for AVs under severe driving conditions (e.g., snowfall) considering the interactions between the AV and surrounding obstacles that have uncertain behaviors by nature. By taking our approach, it is expected that the AV can make an appropriate decision and track the safe trajectory in real-time when faced with an emergency.

1.1. Literature survey

Most previous studies have mainly focused on the following decision-making, path planning and control to drive safely in emergencies.

Regarding the decision-making strategies, Bayesian networks (Noh, 2019; Wang and Hussein, 2011) have been widely implemented to make an appropriate decision under uncertainties. Moreover, Markov Decision Process (MDP)-based decision-making has also been discussed to improve driving safety and efficiency (Bai et al., 2015). However, MDP requires huge computational complexity when solving an even simple problem. Therefore, several artificial intelligence-based decision-making algorithms have been studied recently. Well-known strategies are Deep Neural Networks (DNN) (Nie et al., 2021; Chai

* Corresponding authors.
E-mail addresses: nguyenduyhung@knu.ac.kr (H.D. Nguyen), mucho@nmotion.co.kr (M. Choi), kyoungsh@knu.ac.kr (K. Han).

https://doi.org/10.1016/j.aap.2023.107305
Received 24 February 2023; Received in revised form 16 July 2023; Accepted 13 September 2023
Available online 22 September 2023

et al., 2022) and Reinforcement Learning (RL) (Cao et al., 2021). By exploring-exploiting traffic surroundings, RL can well solve decision-making problems in uncertain environments, whereas DNN can easily adapt to real-time road conditions.

Several global path-planning algorithms (e.g., Dijkstra, rapidly exploring random trees (RRT), RRT*, and A*) (Zheng et al., 2020; Karaman et al., 2011; Duchoň et al., 2014) have been introduced, and they can detect obstacles and create a safe trajectory. These path-planning algorithms can generate the cost-minimum path; however, they generally require high computational capabilities and are suitable for a mobile robot at a low speed. For passenger vehicle path planning, Pontryagin's maximum principle (PMP) (Kopp, 1962; Kim et al., 2023) is used to optimize the path trajectories. In particular, the optimal cost function is reformulated as the integral of the vehicle jerk and boundary conditions without affecting the vehicle stability, which yields safe collision-avoidance trajectories.

Regarding vehicle control systems, they should follow a predefined safe trajectory while maintaining vehicle stability. A neural network-based adaptive path tracking control scheme (Zhihong et al., 1998) is employed to learn the uncertain bounds, and it shows satisfactory tracking performance with the unknown dynamics for nonlinear systems. A traditional proportional–integral-derivative (PID) controller for tracking trajectory (Beck et al., 2023) has a simple structure, easy implementation, and considerable performance of tracking. However, PID lacks the ability to handle constraints. In another study, based on minimizing yaw dynamics, different speed trajectories are compared, and an optimal path is generated (Berntorp et al., 2014). In addition, the vehicle platoon in a lane-changing case is developed using the sliding mode control considering the vehicle longitudinal and lateral dynamics coupling (Ying et al., 2014). In recent decades, a model predictive control (MPC) has been employed to improve tracking performance while considering state and control constraints (Bemporad and Morari, 1999; Deng et al., 2009). For example, vehicle kinematics is assumed to be a linear model, and it tracks the given trajectory accurately at a low-speed (Pereira et al., 2017). The challenges that occur at high speeds have been solved using an accurate dynamics model that achieves satisfactory tracking performance while maintaining stability at a relatively high speed (Kritayakirana and Gerdes, 2012).

For collision avoidance systems, MPC is widespread. Specifically, in Wang and Liu (2022), Chen and Zhang (2022) and Lee and Choi (2022), an LTV-MPC integrated with a conventional A* algorithm to avoid collisions has been introduced, and the road friction coefficient and dynamic pedestrian are considered using a novel long short-term memory (LSTM) algorithm, especially, under slippery road conditions. Although these approaches have achieved high performance in both tracking efficiencies and stability, they cannot avoid the drawbacks of computational burden and the necessity of big datasets when employing the A* and LSTM algorithms.

Further, during path generation, the surrounding environment should be considered to avoid full-blown conflicts. To solve this problem, an artificial potential field (APF) approach (Yue et al., 2021; Nguyen et al., 2023) is widely used to characterize road obstacles and structures (i.e., the number of lanes and road margin) in a 3D map. Additionally, as studied before (Zhang et al., 2017; Ma et al., 2023), the finite state machine (FSM) is a promising method by giving reliable actions through transition conditions.

Motivated by the above previous studies, this paper proposes to use LTV-MPC for vehicle control (Rajamani, 2011), and FSM is efficiently used to make decisions normal and emergency drivings compared with two conventional decision-making approaches, i.e., conventional FSM-based and APF-based highway driving control strategies. The path planning algorithm is comprehensively optimized considering the interactions with the surrounding objects and ride comfort. Additionally, the AV ensures safe driving quality by preventing rear-end car conflicts through evaluating the level of risk in two safety-critical indicators (i.e., TTC and DRAC) (Zhang et al., 2023; Das et al., 2022). Then, using the kinematics through the TTC value (Oberfeld et al., 2022), the navigation function is activated to select a viable safe zone located on road shoulders.

1.2. Contributions

The core contributions of this study are as follows:

(1) We propose a real-time safe path planning trajectory based on the PMP considering the obstacles expressed by the APF. Once the path is determined, its safety is further verified through the receding-horizon control manner that slightly modifies the path to reflect the changed driving conditions, including the uncertainties of interacting vehicles. Also, FSM and Rule-based approaches are combined to give the appropriate vehicle behaviors in real-time, which is improved when compared with conventional FSM-based driving control and APF-based driving strategy. This integrated decision-making procedure is distinguished from the existing studies that focus only on individual features.

(2) We propose adaptive decision-making and control methods that are robust against uncertain driving conditions. For example, the AV consistently searches for a proper safe zone while preventing rear-end car conflicts based on the driving behaviors of interacting vehicles in the next lanes, and makes the decision from the probability of the collisions (i.e., TTC and DRAC). In this manner, automatic decision-making and control methods in emergency situations are developed, and their effectiveness is demonstrated through case studies.

(3) In general, the integration of optimal decision-making and control strategies increases computational complexity, which prevents real-time implementation. To overcome this, we relax the computational burden using the relatively simple FSM-based decision-making approach, and the LTV-MPC is proposed rather than nonlinear MPC, which is usually computationally expensive.

1.3. Paper organization

The remainder of this paper is organized as follows: In Section 2, system modeling for vehicle kinematics and dynamics is introduced. The treated problem is formulated in Section 3. Section 4 proposes risk-informed decision-making and path planning algorithms, whereas in Section 5, the central part of the proposed control method is addressed (i.e., MPC-based vehicle lateral control and PID-based vehicle longitudinal control). In Section 6, the proposed approach's effectiveness is verified through case studies. Finally, Section 7 presents our conclusions of this study.

2. System modeling

2.1. Vehicle kinematics model

A vehicle kinematics model is generally employed at low speed, where the tire force is not involved. The equations of motions are as follows Pereira et al. (2017).

$$\dot{X} = \dot{x}\cos(\psi + \beta), \tag{1a}$$

$$\dot{Y} = \dot{x}\sin(\psi + \beta), \tag{1b}$$

$$\dot{\psi} = \frac{\dot{x}\cos(\beta)}{(l_f + l_r)}\tan\left(\delta_f\right), \tag{1c}$$

where $\dot{X}$ and $\dot{Y}$ denote the global longitudinal and lateral velocities, $\dot{x}$ denotes the longitudinal velocity, ψ and β denote the yaw angle and side slip angle, respectively, l_f and l_r denote the length between the vehicle's center of gravity and the front and rear wheels, respectively, and δ_f denotes the front steering wheel angle.

The state variables for above nonlinear model can be augmented as follows.

$$\dot{\xi}_\kappa(t) = \frac{d\xi_\kappa(t)}{dt} = f_i\left(\xi_\kappa, u, t\right), \qquad \forall i = \{1,2,3\}, \tag{2}$$

where κ denotes kinematics, $\xi_\kappa(t)$ is the state variable (i.e., X, Y, ψ) and $u(t) = \delta_f(t)$ is the control input.

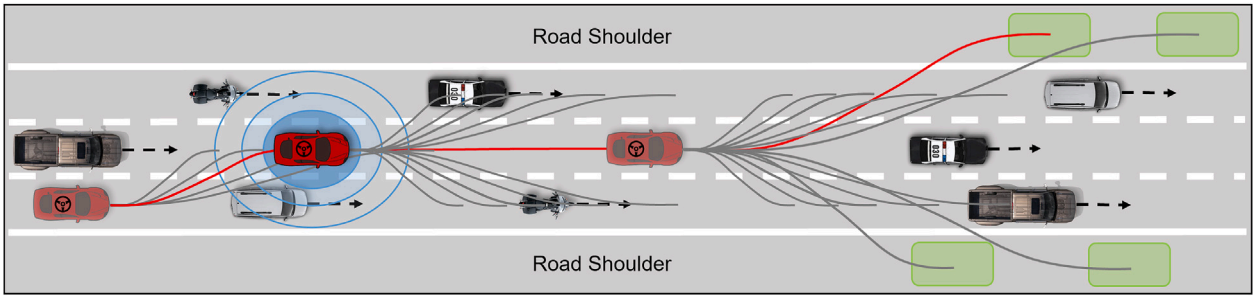

Fig. 1. Example of behavior sequence of AV in an emergency in a mixed-traffic environment.

2.2. Vehicle dynamics model

In this subsection, the vehicle dynamics model is introduced; it has been extensively used in many existing studies (Fuchshumer et al., 2005; Schramm et al., 2014).

Based on the relationship between the force and moment balances, the vehicle's longitudinal, lateral, and yaw dynamics are described as follows.

$$m\ddot{x} = m\dot{y}\dot{\psi} + 2F_{xf} + 2F_{xr}, \tag{3a}$$

$$m\ddot{y} = -m\dot{x}\dot{\psi} + 2F_{yf} + 2F_{yr}, \tag{3b}$$

$$I_z\ddot{\psi} = 2l_fF_{yf} - 2l_rF_{yr}, \tag{3c}$$

where m and I_z denote the total mass and vehicle inertia, respectively, $\ddot{x}$ and $\ddot{y}$ denote the vehicle's longitudinal and lateral accelerations, $\dot{y}$ denotes the lateral velocity, F_x and F_y denote the tire forces about longitudinal and lateral directions, and the subscripts f and r denote the front and rear.

The longitudinal and lateral tire forces, which can be formulated under the assumption of a small front-steering angle, are calculated through the linear tire model ($F_{yf} = C_{\alpha f}\alpha_f$ and $F_{yr} = C_{\alpha r}\alpha_r$; $F_{xf} = C_{\lambda f}\lambda_{xf}$ and $F_{xr} = C_{\lambda r}\lambda_{xr}$). Therefore, by simplifying the dynamics equations (3), the nonlinear vehicle dynamics can be expressed as follows Rajamani (2011).

$$\begin{aligned} m\ddot{y} = {} & 2C_{\alpha r}\frac{l_r\dot{\psi} - \dot{y}}{\dot{x}} + 2C_{\lambda f}\lambda_{xf}\delta_f \\ & - m\dot{x}\dot{\psi} + 2C_{\alpha f}\left(\delta_f - \frac{\dot{y} + l_f\dot{\psi}}{\dot{x}}\right), \end{aligned} \tag{4a}$$

$$\begin{aligned} m\ddot{x} = {} & m\dot{y}\dot{\psi} + 2C_{\lambda f}\lambda_{xf} + 2C_{\lambda r}\lambda_{xr} \\ & - 2C_{\alpha f}\delta_f\left(\delta_f - \frac{\dot{y} + l_f\dot{\psi}}{\dot{x}}\right), \end{aligned} \tag{4b}$$

$$\begin{aligned} I_z\ddot{\psi} = {} & 2l_fC_{\lambda f}\lambda_{xf}\delta_f - 2l_rC_{\alpha r}\frac{l_r\dot{\psi} - \dot{y}}{\dot{x}} \\ & + 2l_fC_{\alpha f}\left(\delta_f - \frac{\dot{y} + l_f\dot{\psi}}{\dot{x}}\right), \end{aligned} \tag{4c}$$

where $C_{\lambda f}$ and $C_{\lambda r}$ denote the stiffnesses following the x-axis of the front and rear tires, λ_{xf} and λ_{xr} denote the front and rear slip ratios of the wheels, which are assumed to be known under the assumption of the constant vehicle speed, $C_{\alpha f}$ and $C_{\alpha r}$ denote the cornering stiffnesses at the front and rear wheels, and α_f and α_r denote the tire side slip angles at the front and rear axles.

Based on the kinematic and dynamic equations (i.e., (1) and (4)), the following nonlinear augmented system model can be defined:

$$\dot{\xi}_a(t) = \frac{d\xi_a(t)}{dt} = f_i\left(\xi_a(\mu), u, t\right), \qquad \forall i = \{1, \ldots, 6\}, \tag{5}$$

where a refers to the augmented model, μ is the road-friction coefficient, $\xi_a(t) = [\xi_d(t), \xi_\kappa(t)]^\top$ are the state variables (i.e., $\dot{y}, \dot{x}, \psi, \dot{\psi}, Y, X$), where d denotes dynamics.

Here, we assume that the road friction coefficient is given based on the several estimation approaches (Han et al., 2017).

3. Problem formulation

The goal of this study is to prevent collisions between the AV and static/dynamic obstacles on slippery roads through the appropriate sequential steering and braking operations. The probabilities of collisions with each interactive vehicle are evaluated in real-time, and a safe optimal path is generated so that the AV arrives at a specific safe zone located on the road shoulder or similar in the end, in case of an emergency situation.

Our approach can be adapted to various driving situations, particularly those involving low road adhesion surfaces and specific road structures. These scenarios may include road shoulders located on either the left or right side or even on both sides of the road. In this, we focus on illustrating an example situation where road shoulders exist on both sides of the road. In such situations, our hierarchical decision-making and control scheme guides the vehicle to move toward a predetermined safe zone that is specific to the given circumstances.

An example of behavior sequences of the AV is illustrated in Fig. 1 when the AV drives in a mixed traffic stream, in which HVs and the AV coexist, especially on the slippery road; thus, many unexpected events can occur. First, the AV changes lanes to avoid a collision that is expected to occur with the vehicle in front while maintaining its yaw stability on the slippery road. After avoiding the collision, we assume that the emergency situation continues due to unexpected obstacles in the middle lane. Depending on the location of the obstacles in the middle lane, the AV should make the following decisions: **(i)** stop immediately in the middle lane if no obstacle is observed in front or **(ii)** determine and move to a safe zone located on the road shoulder, which is a common sequence of actions that should be considered when the vehicle encounters the successive obstacles. Moreover, since the road surface is slippery, both the tracking and vehicle lateral stability should be considered simultaneously.

Specifically, under normal driving conditions, the AV drives based on the FSM logic that includes the states required for highway driving. In case of a risky situation, a safe trajectory is optimally chosen and the AV follows this path while maintaining stability. If these automatic sequential decision-making and control strategies become available for AVs, they are expected to drive safer and more comfortably than human-drivers under harsh driving conditions, which is a major purpose of the proposed method in this study.

4. Risk-informed decision-making and path planning

4.1. FSM-based highway driving

In this study, we assume that the AV drives on highways based on the FSM method regardless of the emergency level. That is, the states and mode switch conditions in FSM should include all possible vehicle behaviors and decisions on the highway.

In the FSM approach (Zhang et al., 2017), a tuple $(s(t), n(t), n_o, i(t))$ is defined, where $s(t)$ denotes the input traffic state (i.e. relative speed and distance between the AV and surrounding vehicles), $n(t)$ denotes the

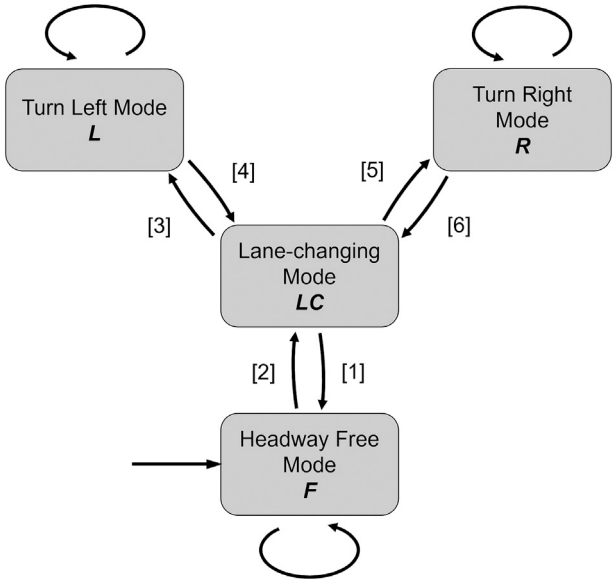

Fig. 2. Diagram for the deterministic FSM-based highway driving control systems.

node-set (i.e., state set), n_o is the initial node, and $i(t) : n(t) \times s(t) \rightarrow n(t)$ represents the state transition function.

Fig. 2 describes a proposed diagram for FSM-based highway driving control. The mode switching occurs deterministically that obeys the policy (π) as follows.

$$[i] = \pi(s(t)), \qquad \forall i = \{1, \dots, 6\}, \tag{6}$$

where $[i]$ denotes the state transition conditions.

The employed states themselves and the state transition conditions are described below.

$$[1], \text{ if } s(t): x^{\text{fl}}_{\text{obs}} - x > d_{\text{far}}, \tag{7a}$$

$$[2], \text{ if } s(t): \begin{cases} x - x^{\text{rl}}_{\text{obs}} \le d_{\text{far}} \text{ or } x^{\text{fl}}_{\text{obs}} - x \le d_{\text{far}}, \\ \text{and} \\ \dot{x} < \dot{x}^{\text{rl}}_{\text{obs}} \text{ or } \dot{x} > \dot{x}^{\text{fl}}_{\text{obs}}, \end{cases} \tag{7b}$$

$$[3], \text{ if } s(t): \begin{cases} \text{TTC}_{\text{l}} > \text{TTC}_{\text{r}}, \\ \text{and} \\ \dot{x} \ge \dot{x}^{\text{rt}}_{\text{obs}} \text{ and } \dot{x} \le \dot{x}^{\text{ft}}_{\text{obs}}, \end{cases} \tag{7c}$$

$$[4] = [6], \text{ if } s(t): \begin{cases} \text{TTC}_{\text{l}} = \text{TTC}_{\text{r}}, \\ \text{and} \\ \dot{x} \ge \dot{x}^{\text{rt}}_{\text{obs}} \text{ and } \dot{x} \le \dot{x}^{\text{ft}}_{\text{obs}}, \end{cases} \tag{7d}$$

$$[5], \text{ if } s(t): \begin{cases} \text{TTC}_{\text{l}} < \text{TTC}_{\text{r}}, \\ \text{and} \\ \dot{x} \ge \dot{x}^{\text{rt}}_{\text{obs}} \text{ and } \dot{x} \le \dot{x}^{\text{ft}}_{\text{obs}}, \end{cases} \tag{7e}$$

where rl and fl indicate the rear and forward directions located on the same lane with the AV, obs denotes the obstacle. rt and ft denote the rear and forward directions located on the target lanes or adjacent lanes, and d_{far} represents the maximum safe margin.

Further, TTC_{l} and TTC_{r} indicate the TTC values calculated between the AV with surrounding HVs located at the left-side lane and right-side lane as follows Minderhoud and Bovy (2001).

$$\text{TTC}_{\text{l}} = \frac{(x^{\text{left}}_{\text{obs}} - x) - \left(0.5l + 0.5l^{\text{left}}_{\text{obs}}\right)}{\dot{x}^{\text{left}}_{\text{obs}} - \dot{x}}, \tag{8a}$$

$$\text{TTC}_{\text{r}} = \frac{(x^{\text{right}}_{\text{obs}} - x) - \left(0.5l + 0.5l^{\text{right}}_{\text{obs}}\right)}{\dot{x}^{\text{right}}_{\text{obs}} - \dot{x}}, \tag{8b}$$

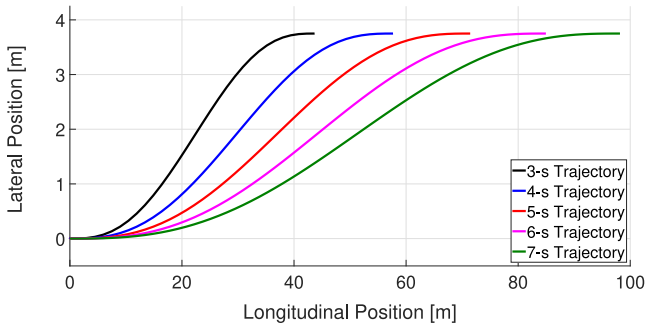

Fig. 3. Lane change trajectory candidates generated by PMP.

where l and l_{obs} denote the lengths of the AV and the obstacle, respectively.

Meanwhile, when $\dot{x}_{\text{obs}} - \dot{x} \le 1$, the denominator of (8) is approximated to 1 to avoid the infinity value. Besides, in the case of the positive numerator, the negative value of the denominator indicates that no collision is expected if the current velocities for AV and HV are maintained.

4.2. Path planning via trajectory optimization

The PMP-based safe trajectory generation approach (Kopp, 1962; Kim et al., 2023) is employed in this study to minimize the vehicle lateral jerk while maintaining the vehicle stability. In particular, depending on the observed obstacle locations, different trajectory candidates can be optimally created.

The following trajectory optimization problem is formulated:

$$\min_{u(t)} J = \int_{t_0}^{t_f} u^2(t) dt, \tag{9a}$$

s.t.

$$\dot{s}_y(t) = v_y(t), \tag{9b}$$

$$\dot{v}_y(t) = a_y(t), \tag{9c}$$

$$\dot{a}_y(t) = u(t), \tag{9d}$$

where t_0 and t_f denote the initial and final times, which are assumed to be the fixed values, $s_y(t)$ indicates the lateral position, $v_y(t)$ is the lateral velocity, $a_y(t)$ denotes the lateral acceleration, and $u(t)$ indicates the lateral jerk that is used as the control input.

The objective of the formulated optimization problem in (9) is to minimize the vehicle lateral jerk while satisfying the following initial and final boundary conditions, which prevent the collision and vehicle slipping out.

$$s_y(t_0) = 0, \; v_y(t_0) = 0, \; a_y(t_0) = 0, \tag{10a}$$

$$s_y(t_f) = 3.75\,\text{m}, \; v_y(t_f) = 0, \; a_y(t_f) = 0, \tag{10b}$$

By appropriately specifying the initial and final boundary conditions, as shown in Fig. 3, the PMP-based safe path-planning can generate multiple trajectories. In this study, we consider five trajectories based on the vehicle physical limitation on the slippery road.

After initializing the multiple path candidates via PMP, the AV will determine one specific trajectory through the Rule-based safe margin ranges of distance classification of surrounding AV (i.e., near, nominal, and far ranges). As shown in Fig. 4, The safe margin ranges are classified based on the level of the collision risk to AV. The values of these distances are specified by the circles of different diameters (i.e., Close = 40 m, Nominal = 80 m, and Far = 120 m), these are tunable values depending on the vehicle, that are the distances from the center of the AV, which are automatically drawn to determine the

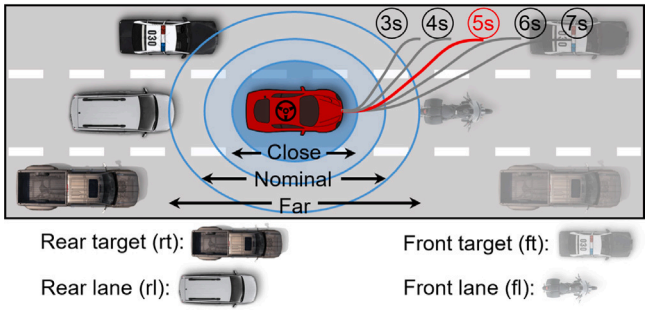

Fig. 4. Safe path trajectory selection via Rule-based safe margin creation.

specific trajectory by comparing the relative distances between the AV and the nearest surrounding HV in the adjacent lane (i.e., $\Delta x_{\mathrm{rt/ft}}$), and depending on the level of emergency, a feasible safe path is chosen based on the following rules:

$$\text{"}3s\text{-path"}, \quad \text{if} \quad \Delta x_{\mathrm{rt/ft}} \in (0, d_{\mathrm{near}}], \tag{11a}$$

$$\text{"}4s\text{-path"}, \quad \text{if} \quad \Delta x_{\mathrm{rt/ft}} \in (d_{\mathrm{near}}, d_{\mathrm{nom}}^{\min}], \tag{11b}$$

$$\text{"}5s\text{-path"}, \quad \text{if} \quad \Delta x_{\mathrm{rt/ft}} \in (d_{\mathrm{nom}}^{\min}, d_{\mathrm{nom}}^{\max}], \tag{11c}$$

$$\text{"}6s\text{-path"}, \quad \text{if} \quad \Delta x_{\mathrm{rt/ft}} \in (d_{\mathrm{nom}}^{\max}, d_{\mathrm{far}}], \tag{11d}$$

$$\text{"}7s\text{-path"}, \quad \text{if} \quad \Delta x_{\mathrm{rt/ft}} \in (d_{\mathrm{far}}, \infty), \tag{11e}$$

where d_{near} and d_{nom} represent the near and nominal safe margins, respectively.

In this intuitive manner, a potential trajectory to follow is determined, and it will be further investigated in the next subsection.

4.3. APF-based optimal trajectory confirmation

After choosing the specific trajectory from the Rule-based approach in (11), the APF approach is further considered to confirm the path considering the location of the dynamic/static obstacles around. Specifically, the optimal control problem is reformulated in a receding-horizon control manner as follows Yue et al. (2021).

$$\min_{u' \in U'} J_{\mathrm{RHC}} = \sum_{k=1}^{N_{p'}} (\|e_Y\|_{Q_1}^2 + \|e_\psi\|_{Q_2}^2) + \sum_{k=0}^{N_{c'}-1} \|u'\|_{R'}^2 + S J_{\mathrm{obs}}, \tag{12}$$

where e_Y, e_ψ, and u' denote the lateral position error and yaw angle error between the vehicle modeling and PMP-based reference, and input signal of planner; Q_1, Q_2, R', and S are weighting matrices correspondingly; Additionally, $N_{p'}$ and $N_{c'}$ denote the prediction and control horizons; J_{obs} indicates the obstacles modeled by APF.

As described in Fig. 5, all interactive obstacles are modeled in the potential field as the form of squared-negative-exponential, which is expressed as follows Nguyen et al. (2023).

$$J_{\mathrm{obs}} = \sum_j A_{\mathrm{obs}} \cdot e^{\left(-\left\{ \frac{\left(x_{\mathrm{glo}} - x_{\mathrm{obs}}^j\right)^2}{2\sigma_x^j} + \frac{\left(y_{\mathrm{glo}} - y_{\mathrm{obs}}^j\right)^2}{2\sigma_y^j} \right\}^c \right)}, \tag{13}$$

where x_{obs}^j and y_{obs}^j denote the jth obstacle's coordinate located on the global map $(x_{\mathrm{glo}}, y_{\mathrm{glo}})$, A_{obs} denotes the maximum value of the potential field model, and c represents the obstacle shape correction factor.

Besides, σ_x^j and σ_y^j are the obstacle potential fields' convergence coefficients as follows.

$$\sigma_x^j = \begin{cases} \min\left\{ \left(\dot{x} - \dot{x}_{\mathrm{obs}}^j\right)^2, \left(x_{\mathrm{glo}} - x_{\mathrm{obs}}^j\right)^2 \right\}, & x_{\mathrm{glo}} \le x_{\mathrm{obs}}^j, \\ \left(l_{\mathrm{obs}}^j + \varepsilon\right)^2, & \text{otherwise}, \end{cases} \tag{14a}$$

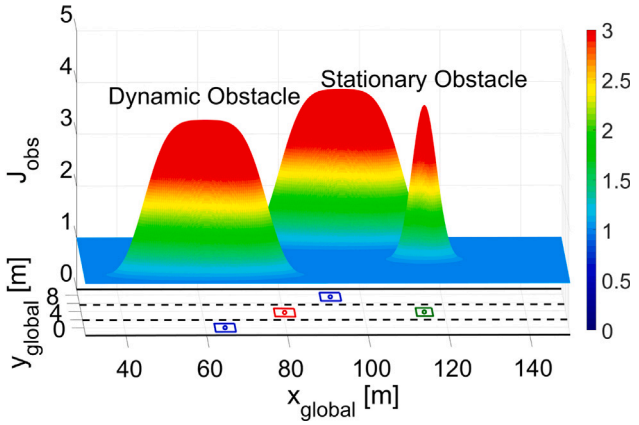

Fig. 5. Obstacle detection in a 3D space.

$$\sigma_y^j = \left(\frac{w_{\mathrm{obs}}^j}{2}\right)^2, \tag{14b}$$

where w_{obs} denotes the width of traffic-road obstacles; and ε indicates a safety factor for covering the AV from the obstacle edges.

In this manner, the specific path selected from the PMP will be used as the reference, and the final path is confirmed through the above receding-horizon control manner. Furthermore, by using optimal control sequence $\left[u'(0), u'(1), \ldots, u(N'_c - 1)\right]^\top$, the receding-horizon control will initialize reference (Y^r) correspondingly, including the lateral position, yaw angle, and yaw rate references, as follows.

$$Y^r = \left[y^r(1), y^r(2), \ldots, y^r(N'_p)\right]^\top, \tag{15}$$

4.4. Safe zone searching

We assume that the AV needs to approach a safe zone (e.g., left/right road shoulder) once it avoids the obstacle. Additionally, two safety level indicators, i.e., the TTC threshold (Thres.) and DRAC threshold ($\mathrm{DRAC}_{\mathrm{Thres.}}$), are employed for evaluating conflicts and selecting the safe zone.

First, the TTC formulation between the AV and jth vehicle in the next lanes is defined as follows.

$$\mathrm{TTC}_j = \frac{(x^j(t) - x(t)) - 0.5\left(l + l_j\right)}{\dot{x}^j(t) - \dot{x}(t)}, \tag{16}$$

Correspondingly, the DRAC is a simple measurement of the highest value at which a vehicle must decelerate to avoid a collision. Besides, the DRAC factor often uses as a safety level indicator to prevent car conflicts in a rear-end collision risk evaluation (Das et al., 2022; Zhang et al., 2023). The DRAC formulation is calculated whenever detecting the j_{lead}^{th} leading obstacle/vehicle, which is expressed in the following Zhang et al. (2023).

$$\mathrm{DRAC}_{j_{\mathrm{lead}}} = \begin{cases} \dfrac{\left(\dot{x}(t) - \dot{x}^{j_{\mathrm{lead}}}(t)\right)^2}{\left(x^{j_{\mathrm{lead}}}(t) - x(t)\right) - 0.5\left(l + l^{j_{\mathrm{lead}}}\right)}, & \dot{x}(t) \ge \dot{x}^{j_{\mathrm{lead}}}(t), \\ 0, & \text{otherwise}, \end{cases} \tag{17}$$

A specified DRAC threshold is defined as an important aspect in determining the severity of a conflict. Besides, our study aims to improve the safe driving of AVs under harsh dash road surfaces at a relatively high speed. Therefore, a high threshold of DRAC is determined and set up as $3\mathrm{m/s}^2$.

As described in Fig. 6, a feasible safe zone is determined by comparing the TTC with the TTC threshold, which is considered in the following situations.

When a forward obstacle is observed, $\mathrm{TTC}_{\mathrm{obs}}$ will be calculated between the AV and an observed obstacle. First, the AV must ensure

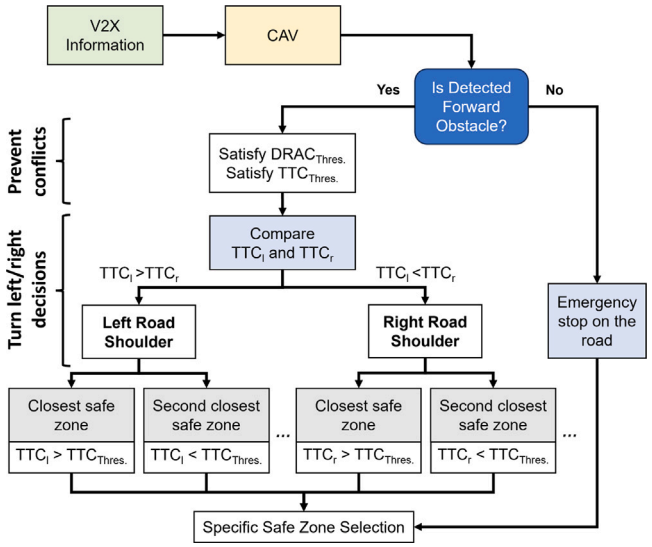

Fig. 6. TTC and DRAC-based the safe zone determination procedure.

that it satisfies the DRAC threshold for preventing car conflicts, then if the TTC_{obs} is less than the TTC threshold, the AV needs to change the lane to avoid collision with this forward obstacle. That is, the AV will determine safe zone candidates on the right and left road shoulders, and then the TTCs calculated between the AV and vehicles right behind in the left and right lanes are compared.

If the TTC_l is higher than TTC_r, the safe zone on the left road shoulder is tentatively determined, and vice versa. Then, the calculated $TTC_{l,r}$ is compared with the threshold (5 s). If the $TTC_{l,r}$ is higher than the threshold, AV chooses the closest safe zone. Otherwise, the AV tries to reach the second closest safe zone, which means that after the interacting vehicle in the next lanes passes the longitudinal position of the closest safe zone first.

Moreover, if no obstacle in front is observed, then the emergency stop is conducted on the road without lane changes. Based on this simple Rule-based strategy, a real-time safe zone searching method is proposed.

5. Integrated lateral and longitudinal vehicle control

5.1. MPC-based vehicle lateral control

The LTV-MPC approach is designed in this study for the optimal solutions with the relaxed computations.

First, to linearize the nonlinear system (i.e., $\xi(t)$ and $u(t)$) of (2) and (5), the nominal point (i.e., $\xi_o(t)$ and $u_o(t)$) is used to obtain the approximated linear model, as follows Falcone et al. (2007), Wang et al. (2016):

$$\dot{\tilde{\xi}}(t) = \frac{d\tilde{\xi}(t)}{dt} = A(t)\tilde{\xi}(t) + B(t)\tilde{u}(t), \tag{18}$$

where $\tilde{\xi}(t) = \xi(t) - \xi_o(t)$ and $\tilde{u}(t) = u(t) - u_o(t)$ denote the state variable and control command errors, respectively, and $A(t)$ and $B(t)$ are the time-varying matrices obtained using the Jacobian, as follows:

$$A(t) = \left.\frac{\partial f_i}{\partial \xi}\right|_{\xi_o(t),u_o(t)}, \; B(t) = \left.\frac{\partial f_i}{\partial u}\right|_{\xi_o(t),u_o(t)}, \tag{19}$$

We discretize the model (18) using Euler approximation theory, as follows.

$$\tilde{\xi}(k+1) = A_d(k)\tilde{\xi}(k) + B_d(k)\tilde{u}(k), \tag{20}$$

where A_d and B_d are the discretized model matrices.

The discretized model (20) is rewritten as the following state deviation:

$$\xi(k+1) = A_d(k)\xi(k) + B_d(k)u(k) + d_o(k), \tag{21}$$

where the deviation $d_o(k) = \xi_o(k+1) - A_d(k)\xi_o(k) - B_d(k)u_o(k)$.

The discretized model (21) is transformed into an augmented model, which is expressed as follows.

$$\begin{aligned} X_{aug}(k+1) &= A_{aug}(k)X_{aug}(k) + \cdots \\ &\quad \ldots + B_{aug}(k)\Delta u(k) + G_{aug}d_o(k), \end{aligned} \tag{22}$$

where the augmented state $X_{aug}(k) = [\xi(k), u(k-1)]^\top$ includes the previous control $u(k-1)$, where $\Delta u(k) = u(k) - u(k-1)$.

According to the augmented model, A_{aug} and B_{aug} denote the augmented matrices as follows:

$$A_{aug}(k) = \begin{bmatrix} A_d(k) & B_d(k) \\ 0 & I \end{bmatrix}, \tag{23a}$$

$$B_{aug}(k) = \begin{bmatrix} B_d(k) \\ I \end{bmatrix}, \; G_{aug} = \begin{bmatrix} I \\ 0 \end{bmatrix}, \tag{23b}$$

We consider the following cost function, which aims to track the trajectory while minimizing the control-rate effort:

$$\begin{aligned} J(\Delta u(t+k|t)) &= \sum_{k=0}^{N_c-1} \|\Delta u(t+k|t)\|_R^2 + \cdots \\ &\quad \cdots + \sum_{k=1}^{N_p} \left\| Y_{aug}(t+k|t) - Y^r(t+k|t) \right\|_Q^2, \end{aligned} \tag{24}$$

where Y^r are the references in dynamics (i.e., lateral position, yaw angle, and yaw rate references) and kinematics (i.e., longitudinal position, lateral position, and yaw angle references), and Y_{aug} denotes the output chosen according to the references. The control signal $\Delta u(t+k|t) = [\Delta u(0|t), \ldots, \Delta u(N_c - 1|t)]$ at time $t+k$ made at time instant t, and Q and R denote the weighting matrices.

The formulation problem is calculated in a receding-horizon control manner, as follows:

$$\min_{\Delta u(0|t),\ldots,\Delta u(N_c-1|t)} J(\Delta u(t+k|t)) \tag{25a}$$

$$\text{s.t} \quad X_{aug}(k+1) = A_{aug}(k)X_{aug}(k) + \cdots \\ \ldots + B_{aug}(k)\Delta u(k) + G_{aug}d_o(k), \tag{25b}$$

$$\Delta u_{\min} \le \Delta u(t+k|t) \le \Delta u_{\max}, \quad \forall k = 0, \ldots, N_c - 1 \tag{25c}$$

$$Y_{aug,\min} \le Y_{aug}(t+k|t) \le Y_{aug,\max}, \quad \forall k = 1, \ldots, N_p \tag{25d}$$

where the prediction horizon N_p is assumed to be equal to the control horizon N_c in this paper.

The linearization points at every time step can be obtained to formulate the LTV-MPC problem in (25). The minimization of the objective function in (25) is treated as a quadratic programming problem (Tøndel et al., 2003).

By solving the above the LTV-MPC problem, the optimized sequence of control can be obtained as follows:

$$\mathcal{U}(t) = \left[\Delta u(0|t), \Delta u(1|t), \ldots, \Delta u(N_c - 1|t)\right], \tag{26}$$

Based on the receding-horizon control, the first element $u(0|t)$ is used to calculate the input signals and others

$$\{\Delta u(1|t), \Delta u(2|t), \ldots, \Delta u(N_c - 2|t), \Delta u(N_c - 1|t)\}, \tag{27}$$

are used to estimate and predict the following augmented state and output sequences at current time t:

$$\mathcal{X}(t) = \left[X_{aug}(1|t+1), \ldots, X_{aug}(N_p|t+1)\right], \tag{28a}$$

$$\mathcal{Y}(t) = \left[Y_{aug}(1|t), \ldots, Y_{aug}(N_p|t)\right], \tag{28b}$$

In this manner, the improved model accuracy for the length of the prediction horizon is realized, resulting in the improved tracking performance, as compared to the invariant model.

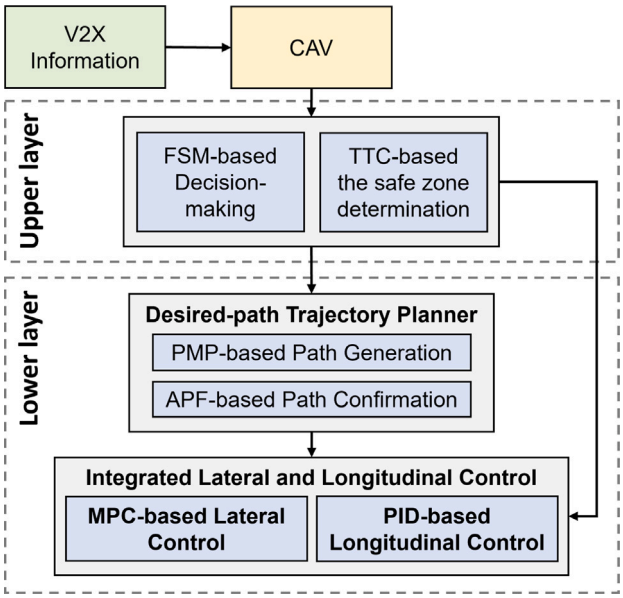

Fig. 7. Hierarchical schematic of proposed integrated decision-making and control algorithms.

5.2. PID-based vehicle longitudinal control

The conditions have been considered in this study focus on AV driving during emergencies; therefore, our aim is to decelerate the AV as quickly as possible without causing any vehicle longitudinal instability. A simple PID control is considered three units of the proportional P, integral I, and derivative D, as follows Ang et al. (2005).

$$u(t) = K_p e(t) + K_i \int_0^t e(\tau) d\tau + K_d \frac{d}{dt} e(t), \tag{29}$$

where τ is the integral variable with a value from 0 to the current time t, $e(\tau)$ is the error value that can be calculated by subtracting the set points (e.g., lane center, and desired speeds) from the output signals. K_p, K_i, and K_d are the tunable coefficients.

5.3. Overall hierarchical structure of proposed method

Fig. 7 illustrates a hierarchical schematic of the proposed integrated decision-making and control strategies for the AV, including the upper layer: FSM-based decision-making and safe zone searching, and the lower layer: path planning/confirmation and longitudinal/lateral vehicle controls.

The CAV drives using a conventional driving policy that relies on the FSM-based decision-making strategy. In the upper layer, when the CAV receives potentially hazardous messages from the V2X technology, the TTC-based safe zone determination procedure is performed. Once it gets the risky messages from the V2X technology, in the upper layer, the TTC-based safe zone is determined by its system. It employs the TTC-based safe zone calculation to determine a safe distance and ensure a secure driving environment.

In the lower layer, the real-time safe path is immediately generated using the PMP approach, while, at the upper layer, the system consistently searches for a safe zone from the local map. Then, based on the APF approach, the generated path by PMP is confirmed. After generating a risk-informed safe optimal path, the vehicle follows it using lateral and longitudinal controls to reach the safe zone. In this manner, the safe and robust decision-making and control methods guide the AV to the safe zone.

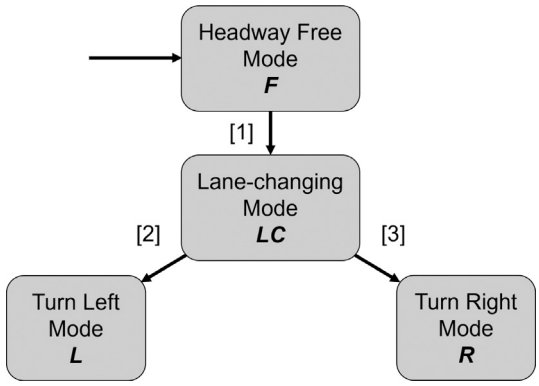

Fig. 8. Conventional FSM-based highway driving control.

6. Simulation tests

We validate the proposed method via a joint simulation using MATLAB/Simulink and CarSim under severe driving conditions (i.e., low-adhesion road $\mu = 0.3$) in the mixed-traffic, where the AV and multiple HVs coexist (video link: https://www.youtube.com/watch?v=KP3GmEMSIIc); besides, the initial velocity of the AV is set relatively high $\dot{x} = 15$ m/s. A computational burden is not observed when the optimal control sequence is searched through the LTV-MPC using the following desktop specifications: 11th Gen Intel(R) Core(TM) i7-11700F @ 2.50 GHz (16 CPUs), ~2.5 GHz, RAM of 32 GB, Windows 10. Additionally, a safe path for a lane change using the PMP theory could be generated in milliseconds.

The effectiveness of the proposed method is investigated in different scenarios, i.e., **Case I:** Normal scenario, **Case II:** Aggressive scenario, **Case III:** More complex scenario, and **Case IV:** Parking on the road.

6.1. Baseline decision-making algorithms

In this subsection, we introduce two alternative baselines, i.e., **(i)** Conventional FSM-based method and **(ii)** APF-based method, used to compare the performance of the proposed method.

6.1.1. Conventional FSM-based decision-making strategy

The conventional FSM-based decision-making strategy is described in Fig. 8, where the decision is made by comparing the relative distances between the AV and the surrounding vehicles.

The transition conditions that determine the driving modes are as follows.

$$[1],\ \text{if } s(t): x_{\text{obs}}^{\text{fl}} - x > d_{\text{far}}, \tag{30a}$$

$$[2],\ \text{if } s(t): \Delta x_{\text{rt/ft}}^{\text{left}} > \Delta x_{\text{rt/ft}}^{\text{right}}, \tag{30b}$$

$$[3],\ \text{if } s(t): \Delta x_{\text{rt/ft}}^{\text{left}} < \Delta x_{\text{rt/ft}}^{\text{right}}, \tag{30c}$$

6.1.2. APF-based decision-making strategy

Another alternative method, namely APF-based safe zone determination, as mentioned in the previous section, APF can further be employed to determine a feasible safe zone location by formulating the magnitude of potential obstacles on the road, i.e., static/dynamic obstacles. Furthermore, as shown in Fig. 9, each goal (i.e., each safe zone location) can also be formulated as follows Ji et al. (2023).

$$J_{\text{goal}} = A_{\text{goal}} \sqrt{\left(x_{\text{goal}} - x_{\text{glo}}\right)^2 + \left(y_{\text{goal}} - y_{\text{glo}}\right)^2}, \tag{31}$$

where A_{goal} denotes the tunable artificial potential gain of the desired point and $(x_{\text{goal}}, y_{\text{goal}})$ features the goal (i.e., safe zone) coordinate, respectively.

Therefore, we can obtain a feasible safe zone by comparing some safe zone's potentials. The possible safe zone is chosen in a way that minimizes the magnitude of potential.

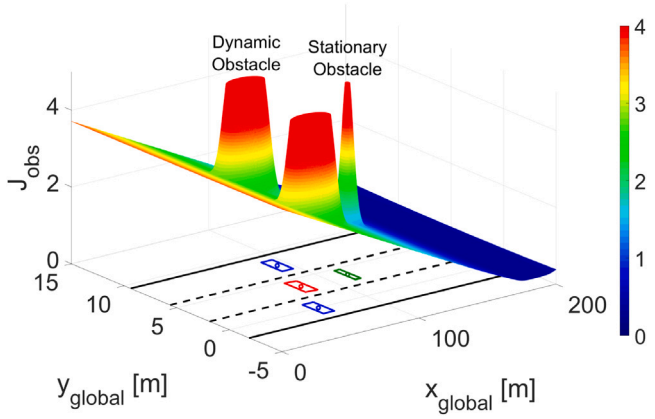

Fig. 9. APF-based decision-making strategy.

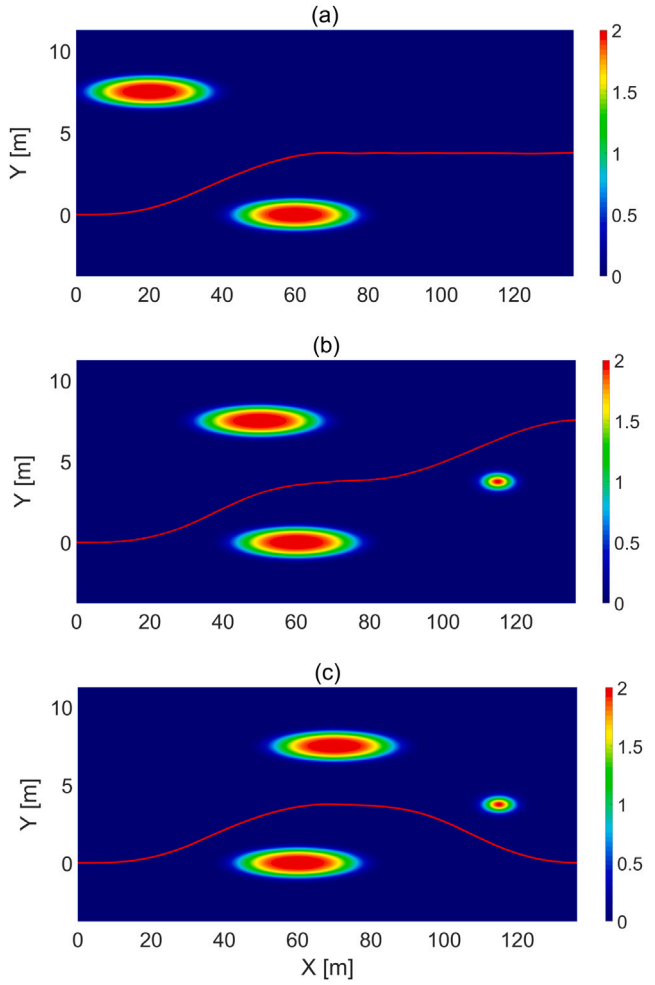

Fig. 10. Three test scenarios: (a) Collision avoidance and stopping; (b) and (c) Collision avoidance and further accident avoidance.

6.2. Results and discussion

We assume the static/dynamic obstacle in front, and it is modeled by the APF approach, as described in Fig. 10; thus, the lane-change maneuver is necessary to avoid a collision. Also, in this verification, we assume that the AV should stop at a certain safe zone due to the sensor failure. Once the AV stops at a certain point, then it alarms its system error to the surrounding vehicles, and it is assumed that they

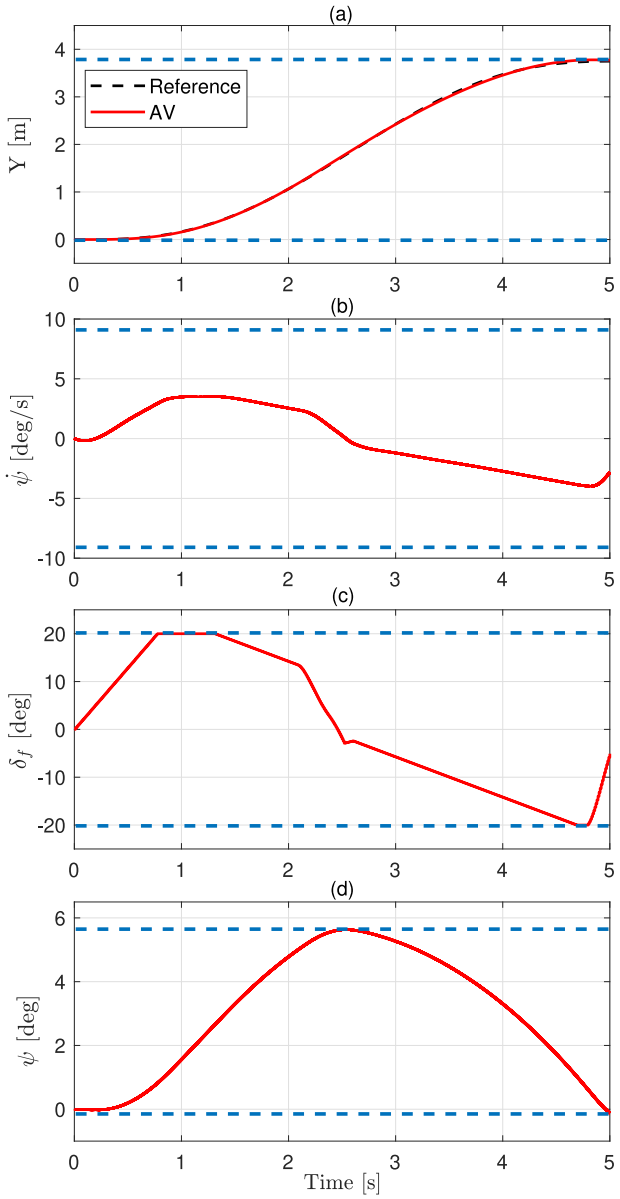

Fig. 11. Path tracking performance for lane-changing maneuver: (a) lateral position, (b) steering wheel angle, (c) yaw rate, and (d) yaw angle, here dashed lines are specified constraints. Here, blue-dashed lines denote the constraints. (For interpretation of the references to color in this figure legend, the reader is referred to the web version of this article.)

avoid the stationary AV well. Therefore, a further collision between the surrounding vehicles and stationary AV is not considered in this study.

In a driving situation shown in Fig. 10(a), a single lane-changing is required and AV can stop in the middle lane since no obstacle is placed, and this risk is assumed to be informed to the AV. By contrast, in the situations described in Fig. 10(b) and (c) the AV needs to avoid a further accident after changing lanes to avoid a collision with the static obstacle placed at the relatively close location in the middle lane. Here, depending on the relative distance and speed to the static obstacle, an appropriate decision to choose a specific safe zone should be made, and our approach is based on the FSM.

Since the road condition and tire model could influence the vehicle stability and tracking abilities, one may argue that control performance will be different when employing the nonlinear tire model as in Jin and Yin (2015). However, we found that no significant difference between when employing linear and nonlinear tire models was observed, so we

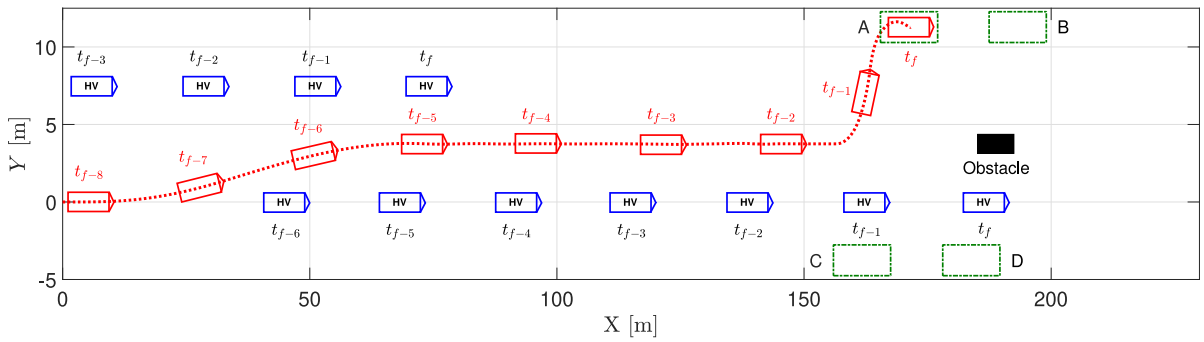

Fig. 12. Vehicle trajectories when AV arrives at the closest safe zone on the left road shoulder.

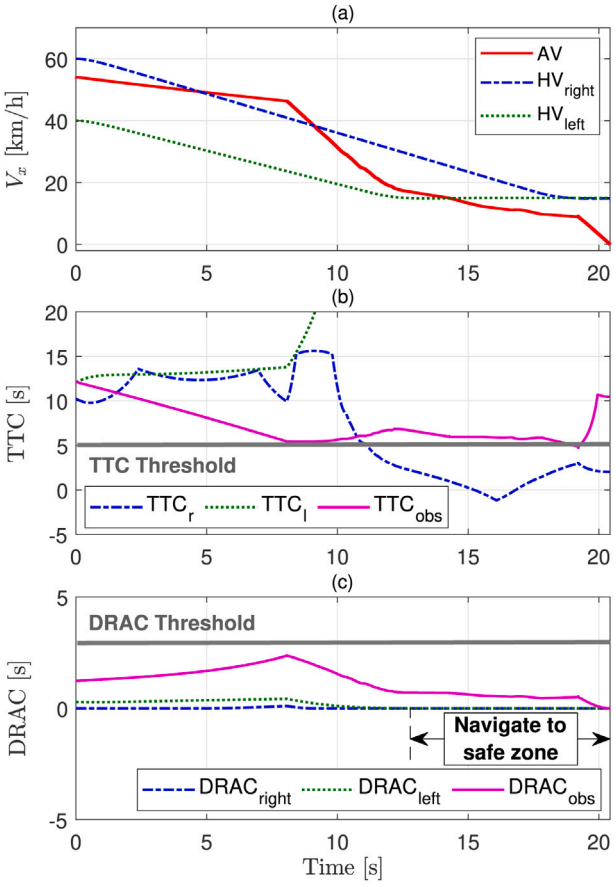

Fig. 13. Test results: (a) Velocity profiles for three interacting vehicles, (b) three TTCs and threshold, and (c) three DRACs and threshold.

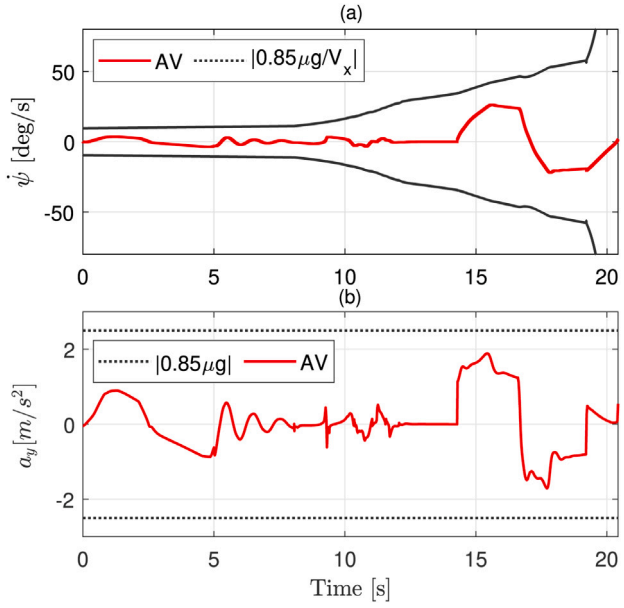

Fig. 14. Vehicle state variables: (a) yaw rate and (b) lateral acceleration.

Table 1
Values of input and state constraints.

Parameter	Y [m]	$\dot{\psi}$ [deg/s]	δ_f [deg]	ψ [deg]	$\Delta\delta_f$ [deg]
Upper bound	3.8	$\dot{\psi}^{\text{bound}}$	20	5.615	9.17×10^{-3}
Lower bound	−0.1	$-\dot{\psi}^{\text{bound}}$	−18	−0.286	-6.59×10^{-3}

adopted the linear tire model to relax the computational complexity in the dynamic situation.

6.2.1. Comparison of decision-making algorithms

For comparison, three decision-making algorithms, i.e., FSM (our approach), conventional FSM, and APF, are simulated in the same environment. Feasible safe zones are determined in specific cases correspondingly, including normal, aggressive, and more complex scenarios.

By using FSM, when considering two safety level indicators (i.e., TTC and DRAC), and formulating artificial potential road objects, FSM and APF can accurately determine the feasible safe zone in all driving cases. However, the conventional FSM-based method sometimes fails to determine the safe zone since it is only based on relative distances (too conservative). Specifically, in the aggressive scenario (case II), surrounding HVs drive aggressively near the AV, i.e., small relative distances, so the AV cannot determine a feasible safe zone.

Additionally, the APF algorithm can determine the feasible safe zone with high accuracy and reasonableness when selecting a safe zone with the lowest cost function value. However, as formulated in Eqs. (13) and (31), depending on the magnitudes of potentials (i.e., static/dynamic obstacles and goals) that can be tuned, there is no explicit difference between safe zones when employing APF, so it is hard to select one.

6.2.2. Collision avoidance

In this subsection, we particularly verify the AV's ability to avoid a collision as soon as the possibility of the collision is informed when employing the proposed methods (i.e., decision-making, and path planning and tracking).

The optimized safe trajectory from the PMP and APF approaches is followed by the LTV-MPC with satisfactory tracking performance, while satisfying the constraints, as shown in Fig. 11(a). The input and state constraints, which can be slightly adjusted for suitable adaptations to handle the tracking performance as well as the vehicle's stability

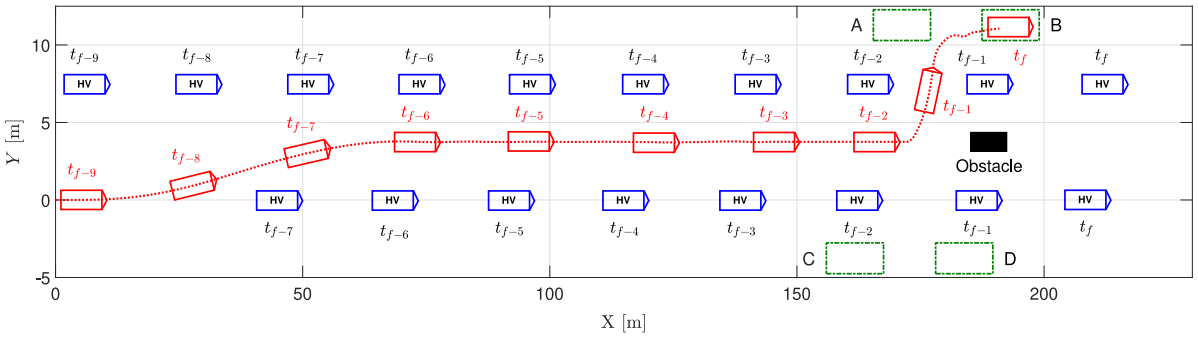

Fig. 15. Vehicle trajectories when AV arrives at the second closest safe zone on the left road shoulder.

in various scenarios, presented in Table 1, are specified considering the physical limitation of the vehicle model and road surface conditions, and the excessive control input is also avoided to prevent the vehicle slipping out. Since the AV drives on a slippery road, somewhat conservative constraints are specified to maintain lateral stability. Appropriate magnitudes for these constraints are found through trial-and-error, and the vehicle slipping out is not observed.

As shown in Fig. 11(a), the vehicle follows the given reference with little deviation, and Fig. 11(b) and (d) show that the vehicle yaw stability is satisfied. Other test results involve various shapes of reference paths depending on the positions of the obstacle in front as all results show similar trends with satisfactory tracking and stability performances. Therefore, it is concluded that the real-time safe path generation through PMP theory and path tracking using the LTV-MPC is feasible at least at the simulation level.

6.2.3. *Safe zone determination*

In this subsection, we verify the effectiveness of the integrated decision-making and control methods, in which the AV adaptively searches the safe zone by evaluating the level of risk and how it reaches the determined safe zone safely under uncertainties. After changing lanes, as verified in the previous subsection, it is assumed that a fixed obstacle is placed relatively close to the AV in the middle lane, and the existence of this obstacle is informed to AV. Therefore, searching and approaching a safe zone on the road shoulder is necessary, which underlines the effectiveness of our approach according to the traffic situations.

In the normal scenario (case I), Fig. 12 depicts the decision-making and control performances when the AV chooses and moves to safe zone A using the LTV-MPC as well as the PID-based longitudinal control. Here, t_f denotes the final simulation time. We can see a large distance between the AV and HV_{left} when compared with the distance between the AV and HV_{right}. Therefore, choosing the left side safe zone seems reasonable, and, due to the enough distance between AV and HV_{left}, the AV chooses safe zone A based on the calculated TTC, rather than safe zone B.

Fig. 13(a) illustrates the velocities of the AV and interacting vehicles, which indicates that HV_{left} drives at a low speed, resulting in the large distance gap, while the AV and HV_{right} drive at a similar velocity. Therefore, as shown in Fig. 13(b), through the TTCs, the interactions between the AV and HVs in the next lanes indicate that the TTC_{l} is greater than the TTC_{r}, which leads the AV to determine the left-side safe zones potentially. Especially, in Fig. 13(c), by satisfying the DRAC threshold, the AV drives without any car rear-end conflicts on highways. Moreover, because of selecting the left-side safe zones, the TTC-left value in the period of the decision has satisfied the TTC threshold (5 s) in Fig. 13, so the closest safe zone on the left road shoulder is chosen. Even if the TTC_{obs} is also larger than the threshold, the stopping at the middle lane is not considered because moving to a safe zone on the road shoulder is given higher priority than other actions in this study.

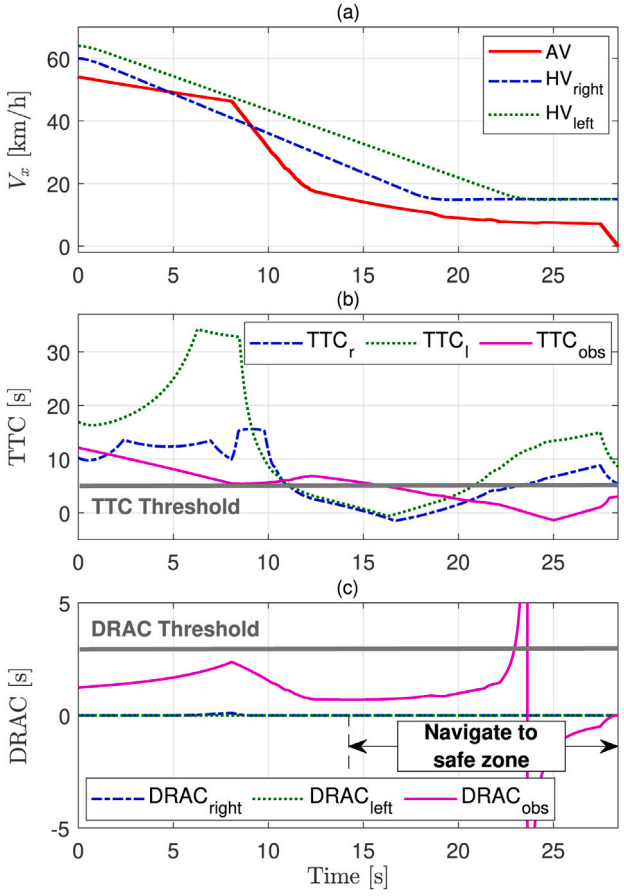

Fig. 16. Test results: (a) Velocity profiles for three interacting vehicles, (b) three TTCs and threshold, and (c) three DRACs and threshold.

Fig. 14(a) and (b) show the yaw rate ($\dot{\psi}(t)$) and lateral acceleration ($a_y(t)$) profiles after lane changing where both satisfy the specified stability thresholds that are a function of the road adhesion μ. The allowable stability threshold standards of these two parameters are the function of μ and V_x as follows Rajamani (2011).

$$|\dot{\psi}| \leq \dot{\psi}^{\text{bound}} = \left|\frac{0.85\ \mu g}{V_x}\right|, \tag{32a}$$

$$|a_y| \leq a_y^{\text{bound}} = |0.85\ \mu g|, \tag{32b}$$

Here, 0.85 is the safety margin.

In the aggressive scenario (case II), Fig. 15 depicts the AV reaching the second closest safe zone on the left road shoulder since the interacting vehicle on the left lane does not allow the lane change. At the time t_{f-1}, the AV begins to change the lane, whereas HV_{left} has

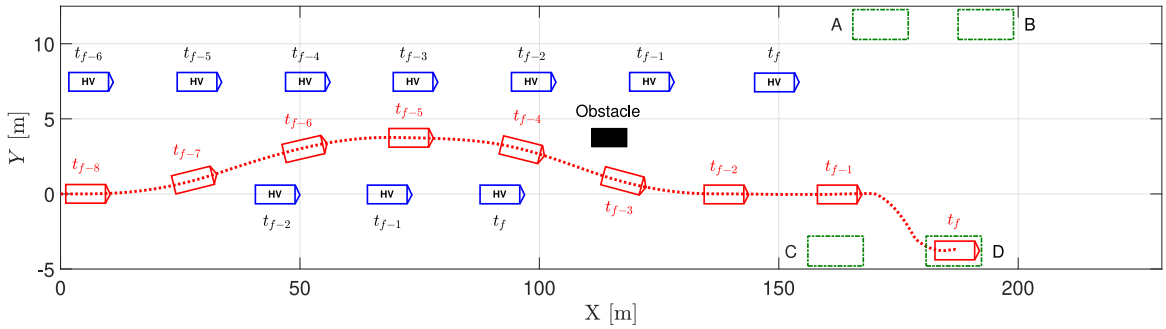

Fig. 17. Vehicle trajectories when AV arrives at the second closest safe zone on the right road shoulder.

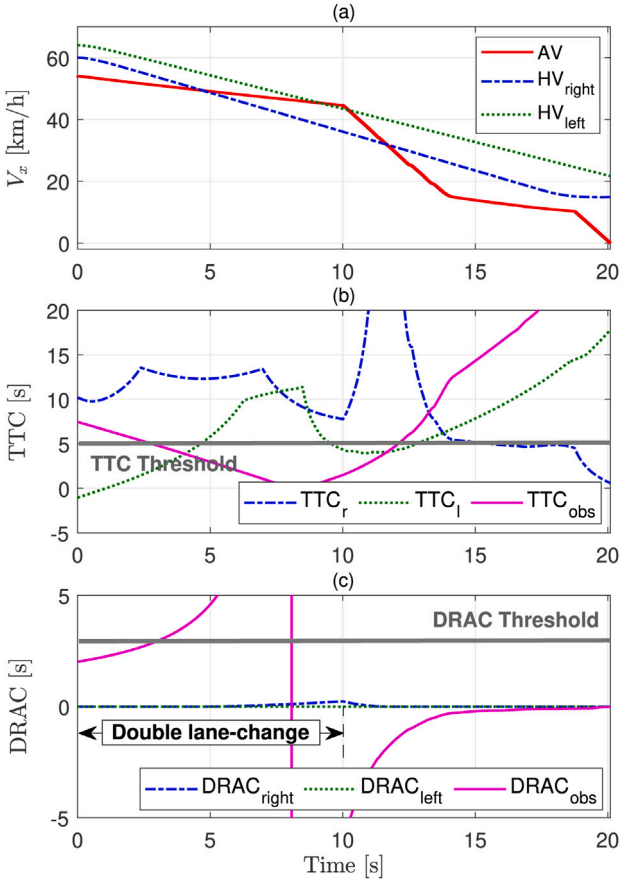

Fig. 18. Test results: (a) Velocity profiles for three interacting vehicles, (b) three TTCs and threshold, and (c) three DRACs and threshold.

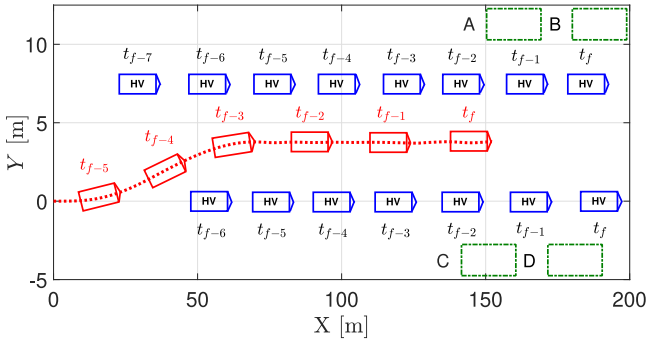

Fig. 19. Vehicle trajectories when AV stops at the middle lane.

passed the position of safe zones first, which is natural in real-world driving. Tracking accuracy and stability are ensured through parameter constraints using the LTV-MPC, while the PID-based lane-keeping assistance/braking system decreases the AV speed at the middle lane sufficiently, then the AV is kinematically controlled at a low speed.

The AV and interacting vehicles drive at a relatively high speed, as illustrated in Fig. 16(a) and rapidly decreasing TTC_l and TTC_r also indicate that the level of collision risk is higher than that of the previous case. The decision to navigate for the AV (i.e., turn left or right) is determined based on the FSM-based driving policy, which shows that the AV decides to approach the left safe zone ($TTC_l > TTC_r$) once it exceeds the threshold around $20s$ as shown in Fig. 16(b). Additionally, during longitudinal vehicle motion (i.e., without any changing lane actions), the AV always satisfies the DRAC threshold, preventing car rear-end conflicts when detecting the potentially risky preceding vehicle, as depicted in Fig. 16(c). Then, when the TTC is less than the threshold of 5 s, the AV will be conflicted when choosing the nearest safe zone, so the AV has to wait until the interacting vehicle passes first, meaning that TTC_l is greater than the TTC threshold. Thus, the selection algorithm shows that the possible safe zone is ***B*** (the second closest safe zone), located at $190m$. In this verification, the TTC_{obs} is mostly around the threshold, so the stopping at the middle lane is undesirable, even if there is not enough room to change the lane in front of the interacting vehicles in the next lanes.

In the more complex scenario (case III), we assumed that the AV drives in an extremely difficult driving situation where the collision avoidance strategy becomes more complicated, illustrated in Fig. 17. However, the AV has still indicated a high safe driving of the longitudinal vehicle motion in preventing car rear-end conflicts when satisfying the DRAC threshold in Fig. 18(c). As described in Fig. 18(a), the AV and interactive vehicles drive at a relatively high speed, while Fig. 18(b) shows the calculated TTC values between the AV and surrounding objects, including HVs and obstacles. After a single lane change to avoid a dynamic obstacle, the TTC_{obs} value indicates a lower value when compared to the threshold (5 s). In this situation, the AV quickly moves back to the original lane considering the evaluated TTCs between the vehicles in both lanes, and chooses the second closest safe zone since the distance between the AV and the closest safe zone is too close after lane-changing. In this case, if the speed of HV_{right} is slightly faster than now, the lane changing to the right lane is not allowed, then the accident mitigation should be considered. This further decision-making for the accident mitigation is left to our future work.

In the final scenario (parking on the road - case IV), we consider the situation when the AV cannot move to any road shoulder since the relative distance and speed between the interacting vehicles are too low to initiate the lane-changing maneuver. Fig. 19 shows the

control/decision performances of the AV when no obstacle is found in the lane, and the "emergency stop on the road" decision is determined. Since the relative speeds of two interactive human-driven vehicles in the next lanes are high, no opportunity to reach the safe zones on the road is provided to the AV in this case. As shown in Fig. 19, AV stops immediately after using the lane-keeping assistance system, and this study does not consider what will happen after the AV stops on the road.

7. Conclusion

In this paper, we propose integrated decision-making and control strategies for the AV in emergency situations, which prevents collisions by satisfying two safety level indicators (i.e., TTC and DRAC) while maintaining the vehicle's lateral stability. Simple FSM-based decision-making is efficiently employed to afford a rough decision according to the driving situations when comparing conventional approaches (i.e., conventional FSM-based and APF-based driving control strategies, and an optimal safe path is generated by using the PMP and APF approaches, which reflect uncertainties in the behaviors of interacting vehicles. The optimal trajectory is followed by the LTV-MPC, which can handle the constraints, and is computationally inexpensive compared with the nonlinear MPC. The effectiveness of our approach is the proposed methods are validated under various traffic conditions, and no computational complexity is found. We believe the proposed methods can help accelerate the development of adaptive decision-making and control, which are essential in the era of autonomous driving. To increase the feasibility of real-time implementation, in our future work, we will implement the developed algorithms on an embedded system and conduct a human-in-the-loop test at the laboratory scale, which will include uncertainties associated with human driving.

CRediT authorship contribution statement

Hung Duy Nguyen: Investigation, Methodology, Visualization, Writing – original draft, Writing – review & editing. **Mooryong Choi:** Writing – review & editing, Methodology. **Kyoungseok Han:** Conceptualization, Funding acquisition, Project administration, Supervision, Writing – review & editing.

Declaration of competing interest

No potential conflict of interest was reported by the author(s).

Data availability

Data will be made available on request.

Acknowledgments

This study was supported in part by the Basic Science Research Program through the National Research Foundation of Korea (NRF), funded by the Ministry of Education (NRF-2021R1A6A1A03043144); in part by the NRF grant funded by the Korean government (MSIT) (NRF-2021R1C1C1003464); and in part by the Technology Innovation Program (20014121, Development of Integrated Minimal Risk Maneuver Technology for Fallback System during Autonomous Driving), funded by the Ministry of Trade, Industry & Energy (MOTIE, Korea).

Appendix A. Supplementary data

Supplementary material related to this article can be found online at https://doi.org/10.1016/j.aap.2023.107305.

References

Ang, K.H., Chong, G., Li, Y., 2005. PID control system analysis, design, and technology. IEEE Trans. Control Syst. Technol. 13 (4), 559–576. http://dx.doi.org/10.1109/TCST.2005.847331.

Bai, H., Cai, S., Ye, N., Hsu, D., Lee, W.S., 2015. Intention-aware online POMDP planning for autonomous driving in a crowd. In: 2015 Ieee International Conference on Robotics and Automation. (Icra), IEEE, pp. 454–460.

Beck, J., Arvin, R., Lee, S., Khattak, A., Chakraborty, S., 2023. Automated vehicle data pipeline for accident reconstruction: new insights from lidar, camera, and radar data. Accid. Anal. Prev. 180, 106923.

Bemporad, A., Morari, M., 1999. Control of systems integrating logic, dynamics, and constraints. Automatica 35 (3), 407–427.

Berntorp, K., Olofsson, B., Lundahl, K., Nielsen, L., 2014. Models and methodology for optimal trajectory generation in safety-critical road–vehicle manoeuvres. Veh. Syst. Dyn. 52 (10), 1304–1332.

Cao, Z., Yang, D., Xu, S., Peng, H., Li, B., Feng, S., Zhao, D., 2021. Highway exiting planner for automated vehicles using reinforcement learning. IEEE Trans. Intell. Transp. Syst. 22 (2), 990–1000. http://dx.doi.org/10.1109/TITS.2019.2961739.

Chai, R., Tsourdos, A., Savvaris, A., Chai, S., Xia, Y., Chen, C.L.P., 2022. Design and implementation of deep neural network-based control for automatic parking maneuver process. IEEE Trans. Neural Netw. Learn. Syst. 33 (4), 1400–1413. http://dx.doi.org/10.1109/TNNLS.2020.3042120.

Chen, H., Zhang, X., 2022. Path planning for intelligent vehicle collision avoidance of dynamic pedestrian using att-LSTM, MSFM, and MPC at unsignalized crosswalk. IEEE Trans. Ind. Electron. 69 (4), 4285–4295. http://dx.doi.org/10.1109/TIE.2021.3073301.

Das, T., Samandar, M.S., Rouphail, N., 2022. Longitudinal traffic conflict analysis of autonomous and traditional vehicle platoons in field tests via surrogate safety measures. Accid. Anal. Prev. 177, 106822.

Deng, J., Becerra, V., Stobart, R., 2009. Input constraints handling in an MPC/feedback linearization scheme. Int. J. Appl. Math. Comput. Sci. 19 (2), 219.

Duchoň, F., Babinec, A., Kajan, M., Beňo, P., Florek, M., Fico, T., Jurišica, L., 2014. Path planning with modified a star algorithm for a mobile robot. Procedia Eng. 96, 59–69.

Falcone, P., Tufo, M., Borrelli, F., Asgari, J., Tseng, H.E., 2007. A linear time varying model predictive control approach to the integrated vehicle dynamics control problem in autonomous systems. In: 2007 46th IEEE Conference on Decision and Control. IEEE, pp. 2980–2985.

Fuchshumer, S., Schlacher, K., Rittenschober, T., 2005. Nonlinear vehicle dynamics control-a flatness based approach. In: Proceedings of the 44th IEEE Conference on Decision and Control. IEEE, pp. 6492–6497.

Han, K., Lee, E., Choi, M., Choi, S.B., 2017. Adaptive scheme for the real-time estimation of tire-road friction coefficient and vehicle velocity. IEEE/ASME Trans. Mechatronics 22 (4), 1508–1518.

Hou, Y., Edara, P., Sun, C., 2015. Situation assessment and decision making for lane change assistance using ensemble learning methods. Expert Syst. Appl. 42 (8), 3875–3882.

Ji, Y., Ni, L., Zhao, C., Lei, C., Du, Y., Wang, W., 2023. TriPField: A 3D potential field model and its applications to local path planning of autonomous vehicles. IEEE Trans. Intell. Transp. Syst. 24 (3), 3541–3554.

Jin, X., Yin, G., 2015. Estimation of lateral tire–road forces and sideslip angle for electric vehicles using interacting multiple model filter approach. J. Franklin Inst. B 352 (2), 686–707.

Karaman, S., Walter, M.R., Perez, A., Frazzoli, E., Teller, S., 2011. Anytime motion planning using the rrt*. In: 2011 IEEE International Conference on Robotics and Automation. pp. 1478–1483. http://dx.doi.org/10.1109/ICRA.2011.5980479.

Kim, D., Nguyen, H.D., Han, K., 2023. State-constrained lane change trajectory planning for emergency steering on slippery roads. IEEE Trans. Veh. Technol..

Kopp, R.E., 1962. Pontryagin maximum principle. In: Mathematics in Science and Engineering, Vol. 5. Elsevier, pp. 255–279.

Kritayakirana, K., Gerdes, J.C., 2012. Using the centre of percussion to design a steering controller for an autonomous race car. Veh. Syst. Dyn. 50 (sup1), 33–51.

Lee, H., Choi, S., 2022. Development of collision avoidance system in slippery road conditions. IEEE Trans. Intell. Transp. Syst. 23 (10), 19544–19556. http://dx.doi.org/10.1109/TITS.2022.3168668.

Ma, Y., Liu, Q., Fu, J., Liufu, K., Li, Q., 2023. Collision-avoidance lane change control method for enhancing safety for connected vehicle platoon in mixed traffic environment. Accid. Anal. Prev. 184, 106999.

Minderhoud, M.M., Bovy, P.H., 2001. Extended time-to-collision measures for road traffic safety assessment. Accid. Anal. Prev. 33 (1), 89–97.

Nguyen, H.D., Kim, D., Son, Y.S., Han, K., 2023. Linear time-varying MPC-based autonomous emergency steering control for collision avoidance. IEEE Trans. Veh. Technol..

Nie, J., Yan, J., Yin, H., Ren, L., Meng, Q., 2021. A multimodality fusion deep neural network and safety test strategy for intelligent vehicles. IEEE Trans. Intell. Veh. 6 (2), 310–322. http://dx.doi.org/10.1109/TIV.2020.3027319.

Noh, S., 2019. Decision-making framework for autonomous driving at road intersections: Safeguarding against collision, overly conservative behavior, and violation vehicles. IEEE Trans. Ind. Electron. 66 (4), 3275–3286. http://dx.doi.org/10.1109/TIE.2018.2840530.

Oberfeld, D., Wessels, M., Büttner, D., 2022. Overestimated time-to-collision for quiet vehicles: Evidence from a study using a novel audiovisual virtual-reality system for traffic scenarios. Accid. Anal. Prev. 175, 106778.

Pande, A., Abdel-Aty, M., 2006. Assessment of freeway traffic parameters leading to lane-change related collisions. Accid. Anal. Prev. 38 (5), 936–948.

Pereira, G.C., Svensson, L., Lima, P.F., Mårtensson, J., 2017. Lateral model predictive control for over-actuated autonomous vehicle. In: 2017 IEEE Intelligent Vehicles Symposium. (IV), IEEE, pp. 310–316.

Rajamani, R., 2011. Vehicle Dynamics and Control. Springer Science & Business Media.

Schramm, D., Hiller, M., Bardini, R., 2014. Single track models. In: Vehicle Dynamics. Springer, pp. 223–253.

Tøndel, P., Johansen, T.A., Bemporad, A., 2003. An algorithm for multi-parametric quadratic programming and explicit MPC solutions. Automatica 39 (3), 489–497.

Wang, Z., Deng, W., Zhang, S., Shi, J., 2016. Vehicle automatic lane changing based on model predictive control. SAE Int. J. Passeng. Cars-Electron. Electr. Syst. 9 (1), 231–237.

Wang, Y., Hussein, I.I., 2011. Bayesian-based decision-making for object search and classification. IEEE Trans. Control Syst. Technol. 19 (6), 1639–1647. http://dx.doi.org/10.1109/TCST.2010.2087760.

Wang, H., Liu, B., 2022. Path planning and path tracking for collision avoidance of autonomous ground vehicles. IEEE Syst. J. 16 (3), 3658–3667. http://dx.doi.org/10.1109/JSYST.2021.3085479.

Ying, Y., Mei, T., Song, Y., Liu, Y., 2014. A sliding mode control approach to longitudinal control of vehicles in a platoon. In: 2014 IEEE International Conference on Mechatronics and Automation. pp. 1509–1514. http://dx.doi.org/10.1109/ICMA.2014.6885923.

Yue, M., Fang, C., Zhang, H., Shangguan, J., 2021. Adaptive authority allocation-based driver-automation shared control for autonomous vehicles. Accid. Anal. Prev. 160, 106301.

Zhang, H., Hou, N., Ding, N., Jiao, N., 2023. Using multicolor perceptual markings as a rear-end crash risk mitigator: A field investigation. Accid. Anal. Prev. 179, 106881.

Zhang, M., Li, N., Girard, A., Kolmanovsky, I., 2017. A finite state machine based automated driving controller and its stochastic optimization. In: Dynamic Systems and Control Conference, Vol. 58288. American Society of Mechanical Engineers, V002T07A002.

Zheng, Z., Wang, Z., Zhu, L., Jiang, H., 2020. Determinants of the congestion caused by a traffic accident in urban road networks. Accid. Anal. Prev. 136, 105327.

Zhihong, M., Wu, H., Palaniswami, M., 1998. An adaptive tracking controller using neural networks for a class of nonlinear systems. IEEE Trans. Neural Netw. 9 (5), 947–955. http://dx.doi.org/10.1109/72.712168.